Dalton Transactions

PAPER

View Article Online
View Journal | View Issue

Cite this: *Dalton Trans.*, 2018, **47**, 7594

Luminescence properties of mechanochemically synthesized lanthanide containing MIL-78 MOFs

Tarek Alammar, *[a] Ihor Z. Hlova,[b] Shalabh Gupta, *[b] Viktor Balema,[b] Vitalij K. Pecharsky[a,b] and Anja-Verena Mudring *[a,b,c]

Received 18th December 2017,
Accepted 23rd April 2018

DOI: 10.1039/c7dt04771a

rsc.li/dalton

Three metal–organic framework (MOF) compounds, $Ln_{0.5}Gd_{0.5}\{C_6H_3(COO)_3\}$; Ln = Eu, Tb, and Dy with a MIL-78 structure, have been synthesized by a solvent-free mechanochemical method from stoichiometric mixtures of benzene 1,3,5-tricarboxylic acid, $C_6H_3(COOH)_3$, also known as trimesic acid, and the respective lanthanide carbonates, $Ln_2(CO_3)_3{\cdot}xH_2O$, Ln = Eu, Gd, Tb and Dy. MIL-78 ($Ln_{0.5}Gd_{0.5}$) shows the characteristic red, green, and yellow luminescence of Eu^{3+}, Tb^{3+}, and Dy^{3+}, respectively. Efficient intramolecular energy transfer from the ligand triplet state to the excited states of Ln^{3+} ions can be observed. The lifetimes and quantum yields of these compounds are studied and discussed in detail. Among the three compounds, the Tb^{3+} containing compound shows the longest lifetime and highest quantum yield due to a smaller contribution from non-radiative decay pathways and better matching of the lowest triplet energy level of the benzenetricarboxylate ligand and the resonance level of Tb^{3+}.

Introduction

Metal–organic frameworks (MOFs) constitute a large class of three-dimensional coordination polymers with ordered microporous structures, which have recently attracted considerable attention as highly promising materials for gas storage and separation, catalysis, magnetic cooling and as luminescent and photonic materials for sensing applications.[1–5] MOFs containing lanthanides (Ln–MOFs) are of particular interest as functional luminescent materials for solid-state lighting and related applications.[4,6] Typically, MOFs are prepared using solution-based techniques including conventional and solvothermal chemical syntheses,[7] as well as less common microwave-assisted,[8] electro-,[9] sono-[10] and liquid-assisted grinding[11] procedures. While solvent-based methods generally produce highly crystalline MOFs, they often rely on hazardous organic solvents and generate considerable amounts of wastes when scaled-up. Among the alternatives, the solvent-free mechanochemical preparation of MOFs, also known as mechanochemistry, has proven to be a rapid, simple and efficient process[12] that is readily adaptable to large-scale production. Mechanochemistry often produces materials with unique particle shapes, sizes, morphologies and structure defects, which can influence or even determine their photoluminescence properties.[13] Therefore, in order to fully establish mechanochemistry as a preferred synthesis route for advanced phosphor materials, it is critical to understand the effects of mechanical processing on the luminescence properties of phosphors. For the application of Ln–MOFs in solid-state lighting, for example, in wLEDs (white light emitting diodes), aside from an efficient emission, a high photoluminescence quantum yield and excellent color purity are important prerequisites. In addition to the desired wavelength emission and high conversion efficiency, achieving enhanced stability at high temperatures while maintaining a narrow emission width is of particular interest.[14] The simplicity of preparation and the cost are important factors to consider, too. In this context, a facile, scalable and reliable synthesis of Ln–MOFs like Ln–MIL-78, $[Ln_{0.5}Gd_{0.5}\{C_6H_3(COO)_3\}]$, is important.

The luminescence properties of lanthanide-based MIL-78 MOFs were first described by Férey group.[15,16] It was found that MIL-78 containing Eu, Tb and Dy exhibits excitation under UV radiation with strong red, green and blue emission, respectively.[14] Other lanthanide metals, including Y, Pr, Nd, Sm, Gd and Er, form isostructural MOFs.[15] However, luminescence studies on materials synthesized mechanochemically are scarce.[17] Recently, several studies showed that MIL-78 can be formed by ball milling starting from lanthanide hydrides or carbonates with trimesic acid.[18,19] Herein, we report a study on the luminescence properties of three MIL-78 MOFs $[Ln_{0.5}Gd_{0.5}\{C_6H_3(COO)_3\}]$; Ln = Eu, Tb, and Dy synthesized using the solid-state mechanochemical approach.

[a]*Department of Materials Science and Engineering, Iowa State University, Ames, IA 50011-2300, USA. E-mail: tarek.alammar@rub.de*
[b]*Ames Laboratory, Iowa State University, Ames, IA 500011-3020, USA. E-mail: shalabh@ameslab.gov*
[c]*Department of Materials and Environmental Chemistry, Stockholm University, Svante Arrhenius väg 16 C, 106 91 Stockholm, Sweden. E-mail: anja-verena.mudring@mmk.su.se*

Experimental

Materials

All chemicals were used without further purification. $Eu_2(CO_3)_3{\cdot}4H_2O$, $Gd_2(CO_3)_3{\cdot}4H_2O$, $Tb_2(CO_3)_3{\cdot}6H_2O$, and $Dy_2(CO_3)_3{\cdot}4H_2O$ were purchased from Alfa Aesar and benzene 1,3,5-tricarboxylic acid, $[C_6H_3(COOH)_3]$, *aka* trimesic acid from Sigma-Aldrich.

Synthesis of $Ln\{C_6H_3(COO)\}_3$

Following a previously published synthesis procedure,[19] lanthanide-based MIL-78 MOFs were prepared by ball milling of benzene 1,3,5-tricarboxylic acid $[C_6H_3(COOH)_3]$ with the respective lanthanide carbonate hydrates $[Ln_2(CO_3)_3{\cdot}xH_2O]$ (Ln = Eu, Gd, Tb, and Dy) in a 2 : 1 molar ratio. In a typical experiment, a total 1 g of the stoichiometric mixture of benzene 1,3,5-tricarboxylic acid and the Ln-metal carbonate hydrate was ball milled in a SPEX 8000 M shaker mill for 2 h in a hardened steel container together with two 12.7 mm and four 6.35 mm grinding stainless steel balls achieving a ball-to-sample ratio close to 18 : 1. The reaction conditions used for the synthesis of MIL-78 were optimized in our previous work.[19] As noted in ref. 19, addition of anhydrous dimethylformamide and dimethyl ether prevented the progress of the reaction and, hence, the formation of any condensed species. The reactions were also carried out in the presence of 1–2 molar equivalents of additional water, but no significant changes in the reaction time or crystallinity of the products were noted. Beyond a certain limit of additional water, a plastic-like product was obtained, which was not characterized further.

Characterization

Powder X-ray diffraction (PXRD). PXRD measurements were carried out on a PANalytical X'PERT powder diffractometer with an Xcelerator detector employing Cu-$K_{\alpha1}$ radiation (λ = 0.15406 nm) in the 2θ range from 5° to 80° with a step size of 0.02°. Thermogravimetric Analysis (TGA) and Differential Scanning Calorimetry (DSC) data were collected at a heating rate of 10 °C min^{-1} from room temperature to 1000 °C using a Netzsch Luxx STA 409 PG.

X-ray photoemission spectroscopy (XPS). XPS measurements were performed in a stainless-steel ultrahigh vacuum chamber (PerkinElmer, model 5500, base pressure <10–10 mbar). XPS measurements were performed on a Physical Electronics 5500 multi-technique system with a standard aluminum source. The analysis spot size was 1 × 1 mm. The samples were mounted on double sided Scotch© tape. The binding energies in the XPS spectra are calibrated against the C-1s signal (284.8 eV) corresponding to adventitious physisorbed carbon dioxide.

Infra-Red (IR) spectroscopy. Attenuated total reflection (ATR) spectroscopy was carried out on an Alpha ATR spectrometer equipped with a diamond crystal (Bruker, Karlsruhe, D). Solid samples were pressed on the crystal with a diamond surface to ensure good contact.

UV-Vis spectroscopy. UV-Vis spectra were recorded at room temperature on a Cary 5000 spectrometer (Varian, Palo Alto, USA) in reflection mode.

Fluorescence spectroscopy. Excitation and emission spectra were recorded at room temperature on a HORIBA Jobin Yvon Fluorolog 3-222 spectrofluorometer, equipped with a 450 W xenon arc lamp and a R928P PMT detector. The decay curve measurements were obtained by using the same instrument operating in phosphorescence mode.

Results and discussion

The PXRD patterns of the as-prepared MOFs are shown in Fig. 1. The products obtained upon ball milling with each combination of lanthanides are isostructural, and their PXRD patterns are in good agreement with the calculated pattern of the MIL-78 (Gd) crystallizing in the monoclinic space group $C2/m$ (no. 12).[15] Because of significant line broadening of the Bragg peaks and extremely low intensities above $2\theta \cong 45°$, the peak shifts expected to arise for the different compounds due to the lanthanide contraction are not discernible. No additional diffraction peaks originating from precursors or other crystalline impurities can be detected confirming the phase purity of the obtained materials. The large background is expected to arise from amorphization of a part of the materials.

The TG-DSC analysis of the as-prepared MIL-78 ($Tb_{0.5}Gd_{0.5}$) shows a two-step weight loss between room temperature and 1000 °C (Fig. 2). The first broad loss with a T_{onset} of ~100 °C finishing close to 330 °C can be assigned to the loss of both

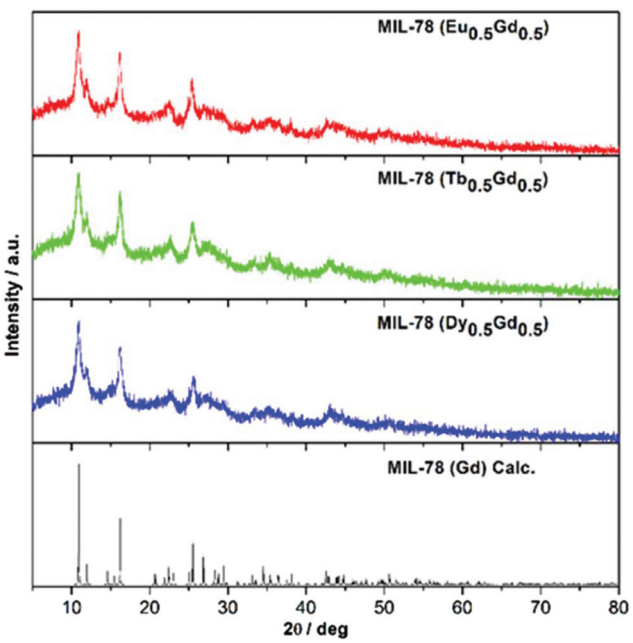

Fig. 1 Powder X-ray diffraction patterns of the mechanochemically prepared MIL-78 ($Ln_{0.5}Gd_{0.5}$) Ln = Eu, Tb, and Dy and the calculated pattern of MIL-78 (Gd).

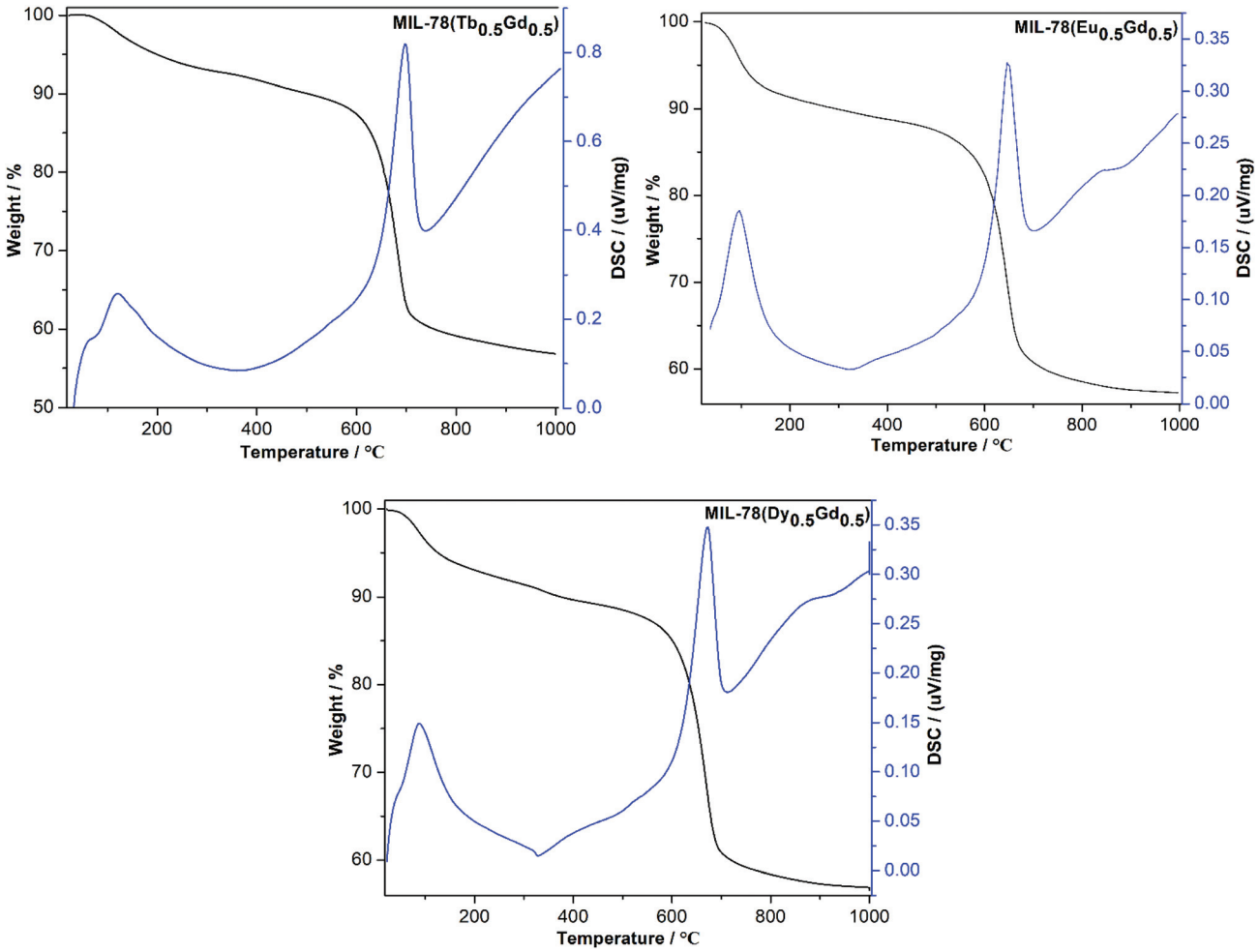

Fig. 2 TG (black line) and DSC (blue line) curves of the as-prepared MIL-78 ($Ln_{0.5}Gd_{0.5}$) Ln = Tb, Eu, and Dy.

physically adsorbed H_2O and the water coordinated within the MIL-78 structure. A similar behaviour is observed for the as-synthesized Eu and Dy containing MIL-78 MOFs (Fig. 2). The weight losses are 10.5% (~3.3 eq. H_2O per f.u.) for the MIL-78 ($Eu_{0.5}Gd_{0.5}$), 7.3% (~2.25 eq. H_2O per f.u.) for ($Tb_{0.5}Gd_{0.5}$), and 9% (~2.8 eq. H_2O per f.u.) for ($Dy_{0.5}Gd_{0.5}$). The second weight loss at a higher temperature with $T_{onset} \cong 600$ °C is attributed to the thermal decomposition of MIL-78 to lanthanide oxides.[15] The thermal behaviours are in agreement with those reported for MIL-78 (Gd), MIL-78 ($Tb_{0.34}Dy_{0.33}Gd_{0.33}$) and MIL-78 ($Dy_{0.5}Gd_{0.5}$).[19] The absence of signals characteristic of trimesic acid and carbonates confirms that all of the precursors reacted, forming desired products.

The surface composition and the oxidation states of the lanthanides in the as-synthesized MIL-78 ($Ln_{0.5}Gd_{0.5}$) Ln = Eu, Tb, and Dy were investigated with X-ray photoelectron spectroscopy (XPS) and the data obtained were analyzed by a curve fitting process shown in Fig. 3. The XPS spectra illustrated in Fig. 3 contain signals that can be attributed to the electronic transitions in Eu, Gd, Tb, Dy, O and C. The Eu-3d, Tb-3d, and Dy-3d scans are presented in Fig. 3. The Eu-3d core-level XPS spectrum in MIL-78 ($Eu_{0.5}Gd_{0.5}$) shows two prominent peaks at 1165.4 eV (Eu^{3+} $3d_{3/2}$) and 1135.4 eV (Eu^{3+} $3d_{5/2}$) with three minor satellites located at 1155.4 eV (Eu^{2+} $3d_{3/2}$), 1143.3 eV (mult), and 1124.8 eV (Eu^{2+} $3d_{5/2}$).

The presence of Eu^{2+} can be attributed to the reduction of Eu^{3+} to Eu^{2+} due to the charge compensation process during profiling under the ambient conditions of XPS measurements which is frequently observed for Eu^{3+} compounds.[20–22] The XPS spectrum for the Tb-3d region of MIL-78 ($Tb_{0.5}Gd_{0.5}$) shows two peaks at 1242.5 eV (Tb^{3+} $3d_{5/2}$) and 1277.2 eV (Tb^{3+} $3d_{3/2}$). A satellite peak observed at 1250 eV is attributed to the presence of Tb^{4+} traces because of the oxidation of Tb^{3+} to Tb^{4+} during the electron beam irradiation, as often observed for the binary oxide and similar compounds when being investigated under similar conditions.[23,24] The two peaks at 1297.5 eV and 1335.4 eV in the XPS spectrum of MIL-78 ($Dy_{0.5}Gd_{0.5}$) can be assigned to Dy^{3+} $3d_{5/2}$ and Dy^{3+} $3d_{3/2}$.[25]

The IR spectra of MIL-78 ($Ln_{0.5}Gd_{0.5}$) with Ln = Eu, Tb, and Dy (Fig. 4) show similar features. The characteristic bands of the protonated carboxyl groups of trimesic acid (νOH, 3085 cm^{-1}; $\nu_{C=O}$, 1714 cm^{-1}; $\delta_{C=O}$, 537 cm^{-1}) and metal car-

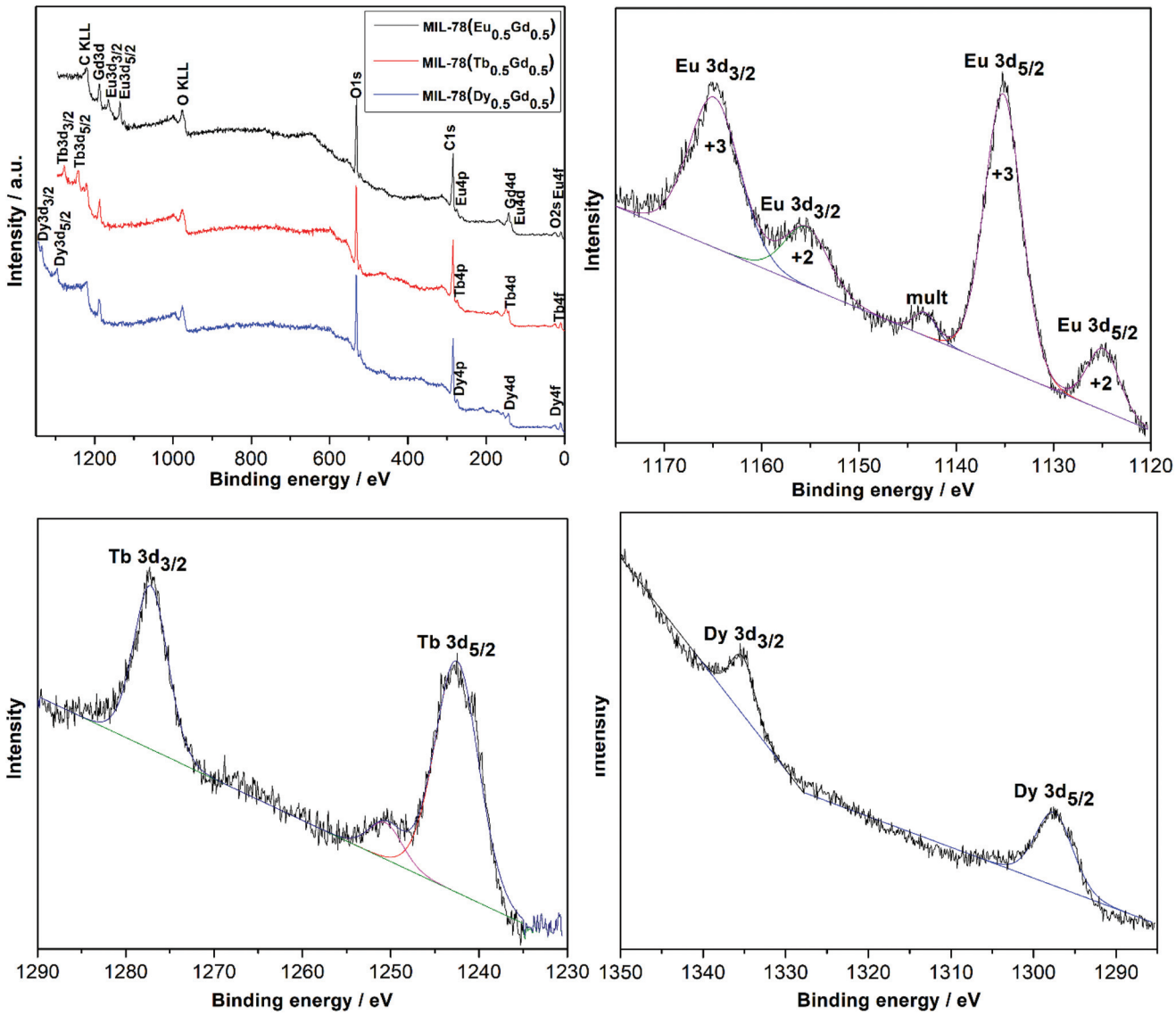

Fig. 3 X-ray photoelectron spectrum survey and narrow scans of Eu-3d, Tb-3d, and Dy-3d regions for MIL-78 ($Ln_{0.5}Gd_{0.5}$) Ln = Eu (black), Tb (red), and Dy (blue).

bonates ($\nu_{C=O}$ between 1500 and 300 cm^{-1}) cannot be observed in the final products which further confirms that the starting materials are fully consumed in the reaction.[26–28] Instead, in the IR spectra of MIL-78 ($Ln_{0.5}Gd_{0.5}$) Ln = Eu, Tb, and Dy, bands at 1542 cm^{-1} and 1357 cm^{-1} which originate from the asymmetric and symmetric C–O stretching vibrations of $-COO^-$, respectively, can be noticed. The value of the difference between ν_{as} and ν_s is about $\Delta\nu$ = 185 cm^{-1}, which indicates that the carboxylate group and metal ions coordinate through a bidentate bridge in the MIL-78 structure.[29] The band located at 759 cm^{-1} can be assigned to the ring-out-of-plane deformation vibration of the benzene core of the substituted trimesic acid. These results confirm the successful coordination of the Ln^{3+} ions with the trimesic acid ligands. Maiti *et al.* reported similar observations for the vibrational spectra of manganese 1,3,5-benzenetricarboxylate MOFs.[30]

UV-Vis absorption spectra of MIL-78 ($Ln_{0.5}Gd_{0.5}$) and trimesic acid (Fig. 5) were recorded in the solid-state at room temperature. As is evident from Fig. 5, MIL-78 ($Ln_{0.5}Gd_{0.5}$) with Ln = Eu, Tb, and Dy show quite similar spectral profiles compared to trimesic acid, suggesting that the complexation of the Ln^{3+} ions does not significantly affect the singlet excitation state of trimesic acid. Starting from high energies, first, the π–π* type of transition in the aromatic ring and then n → π* transitions in the C=O group can be observed.[31,32] In comparison with the transitions in the free trimesic acid, the bands in the absorption spectrum of trimesic acid are red-shifted and additional bands beyond 300 nm are pronouncedly visible. The differences between the absorption spectrum of trimesic acid (H_3BTC) and the spectra of MIL-78 ($Ln_{0.5}Gd_{0.5}$) can be attributed to the deprotonation and coordination of H_3BTC (*i.e.* BTC^{3-}).[33] The f–f transitions of the respective lanthanide

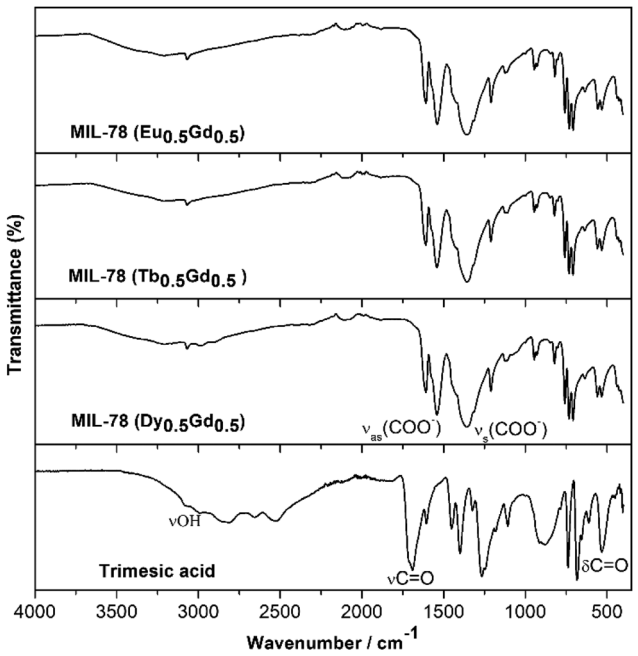

Fig. 4 Infra-red spectra of the as-prepared MIL-78 ($Ln_{0.5}Gd_{0.5}$); Ln = Eu, Tb, and Dy and trimesic acid.

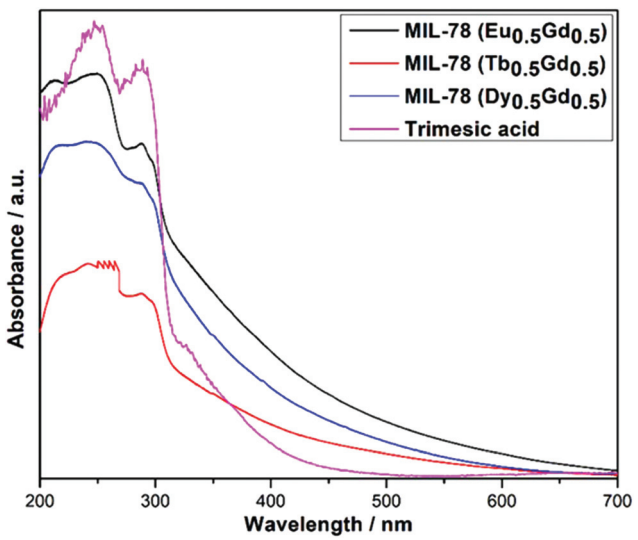

Fig. 5 UV absorbance spectra of MIL-78 ($Ln_{0.5}Gd_{0.5}$); Ln = Eu, Tb, and Dy and trimesic acid.

ions appear to be invisible in the absorption spectrum due to the high intensity of the transitions within the organic moiety, which have a much higher transition probability.

The luminescence properties of three compounds were determined in the solid state at room temperature. Fig. 6 shows the excitation and emission spectra of MIL-78 ($Ln_{0.5}Gd_{0.5}$); Ln = Eu, Tb, and Dy. The excitation spectra were recorded by monitoring the $^5D_0$–$^7F_2$ transition at 613 nm for Eu^{3+}, the $^5D_4$–$^7F_5$ transition at 544 nm for Tb^{3+}, and the $^4F_{9/2}$–$^6H_{13/2}$ transition at 575 nm for Dy^{3+}. Similar to the UV-vis absorption spectra, the excitation spectra of all the samples show broad bands below 300 nm, which can be attributed to the n–π* and π–π* transitions of the ligand, at lower and higher energies, respectively. In addition, the excitation spectrum of MIL-78 ($Eu_{0.5}Gd_{0.5}$) displays peaks with low relative intensities at 362 nm, 394 nm, and 465 nm corresponding to the transitions between the $^7F_0$ ground state and the $^5D_4$, $^5L_6$ and $^5D_2$ excited levels of Eu^{3+}. In contrast, for MIL-78 ($Tb_{0.5}Gd_{0.5}$) no narrow bands arising from 4f–4f transitions characteristic of Tb^{3+} can be observed. This points to an efficient sensitization of Tb^{3+} by the ligand. For MIL-78 ($Dy_{0.5}Gd_{0.5}$), a series of low-intensity bands originating from 4f–4f transitions from the ground state $^6H_{15/2}$ to higher excited states (325 nm ($^6H_{15/2}$–$^6P_{3/2}$ + $^4M_{17/2}$), 351 nm ($^6H_{15/2}$–$^6P_{7/2}$), 365 nm ($^6H_{15/2}$–$^6P_{5/2}$ + $^4I_{11/2}$), 388 nm ($^6H_{15/2}$–$^4I_{13/2}$ + $^4K_{17/2}$), and 454 nm ($^6H_{15/2}$–$^4I_{15/2}$)), were observed. This hints that the 1,3,5-benzenetricaboxylate ligand can sensitize emission of the lanthanide ions, as has been reported previously for Eu- and Tb-benzene-1,3,5-tricarboxylates.[29] Thus, upon excitation to ligand-centered levels below 290 nm, MIL-78 ($Ln_{0.5}Gd_{0.5}$) MOFs show the characteristic emission of Eu^{3+}, Tb^{3+} and Dy^{3+}. The emission spectrum of MIL-78 ($Eu_{0.5}Gd_{0.5}$) displays narrow peaks located at 580, 594, 613, 657.3 and 702.6 nm that can be ascribed to the $^5D_0$–^7F_J (J = 0, 1, 2, 3, and 4) transitions of Eu^{3+}, respectively. The intensity of the hypersensitive $^5D_0$–$^7F_2$ transition is the strongest and responsible for the red luminescence of MIL-78 ($Eu_{0.5}Gd_{0.5}$). No emission from higher excited levels such as $^5D_1$ can be observed, suggesting the efficiency of the non-radiative relaxation to the $^5D_0$ level.

The presence of a $^5D_0$–$^7F_0$ transition agrees with the presence of only one crystallographically independent Eu^{3+} located at a low-symmetry site in the crystal structure of MIL-78.[15] This is also supported by the higher intensity relative to the electric dipole transition $^5D_0$–$^7F_2$ compared to the magnetic dipole transition $^5D_0$–$^7F_1$, *aka* an asymmetry ratio. The full width at half maximum of the most intense band is estimated to be 3.42 nm, which demonstrates that MIL-78 ($Eu_{0.5}Gd_{0.5}$) shows high color purity. It is worth mentioning that the absence of residual emission of the ligand in the range between 400 and 550 nm confirms the efficient intramolecular energy transfer from the ligand to the Eu^{3+} ion. For MIL-78 ($Tb_{0.5}Gd_{0.5}$), typical Tb^{3+} emission bands at 494, 544, 584, 624, 650, 671, and 683 nm are attributed to $^5D_4$–$^7F_6$, $^5D_4$–$^7F_5$, $^5D_4$–$^7F_4$, $^5D_4$–$^7F_3$, $^5D_4$–$^7F_2$, $^5D_4$–$^7F_1$, and $^5D_4$–$^7F_0$ transitions, respectively. The hypersensitive $^5D_4$–$^7F_5$ transition is the most intense among these transitions, and is responsible for its green luminescence (Fig. 6, inset). MIL-78 ($Dy_{0.5}Gd_{0.5}$) also shows typical Dy^{3+} emission bands at 481, 576, and 665 nm due to $^4F_{9/2}$–$^6H_{15/2}$, $^4F_{9/2}$–$^6H_{13/2}$, and $^4F_{9/2}$–$^6H_{11/2}$ transitions, respectively, with the $^4F_{9/2}$–$^6H_{15/2}$ transition (yellow emission) being the most intense.[34] The color coordinates for the as-synthesized MOFs were determined to be (0.64, 0.35) for MIL-78 ($Eu_{0.5}Gd_{0.5}$), (0.30, 0.61) for MIL-78 ($Tb_{0.5}Gd_{0.5}$), and (0.37, 0.417) for MIL-78 ($Dy_{0.5}Gd_{0.5}$) and are shown in the 1931 CIE chromaticity diagram in Fig. 7, which indicates that these

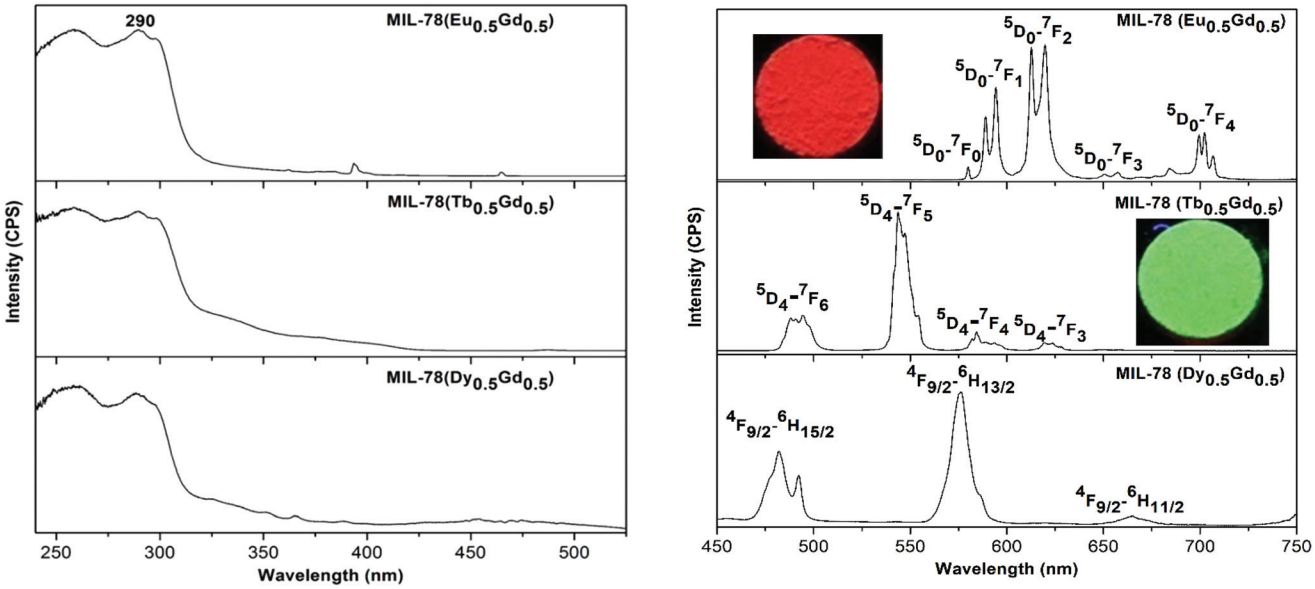

Fig. 6 Excitation (left) and emission (right) spectra of MIL-78 ($Ln_{0.5}Gd_{0.5}$) with Ln = Eu, Tb, and Dy at room temperature. The insets are showing the samples under UV light.

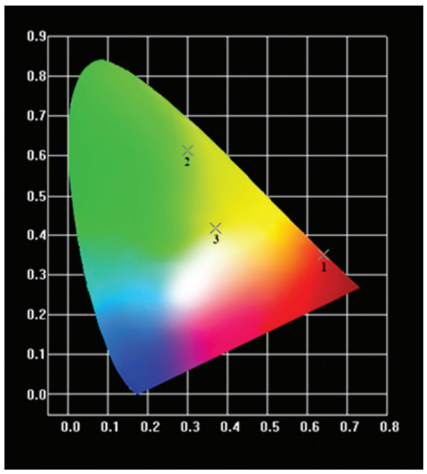

Fig. 7 1931 CIE chromaticity diagram of MIL-78 ($Eu_{0.5}Gd_{0.5}$) (1), ($Tb_{0.5}Gd_{0.5}$) (2), and ($Dy_{0.5}Gd_{0.5}$) (3).

lanthanide-based MOFs can display good color purity for red, green, and yellow emission, respectively. The luminescence decay curves of MIL-78 ($Ln_{0.5}Gd_{0.5}$) Ln = Eu, Tb, and Dy are monitored around the respective strongest emission ($^5D_4$–$^7F_5$ for Tb^{3+}, $^5D_0$–$^7F_2$ for Eu^{3+}, and $^4F_{9/2}$–$^6H_{13/2}$ for Dy^{3+}) at room temperature. The corresponding curves are given in Fig. 8. The curves for MIL-78 ($Eu_{0.5}Gd_{0.5}$) and MIL-78 ($Tb_{0.5}Gd_{0.5}$) are fitted by a single exponential function described using the following equation: $I = I_0 + A_1 \exp(-t/\tau)$. In turn, the curve for MIL-78 ($Dy_{0.5}Gd_{0.5}$) can only be fitted well with a bi-exponential function: $I = I_0 + A_1 \exp(-t/\tau_1) + A_2 \exp(-t/\tau_2)$. The lifetime values are estimated to be $\tau = 0.71 \pm 0.007$ ms for MIL-78 ($Eu_{0.5}Gd_{0.5}$), $\tau = 2.02 \pm 0.02$ ms for MIL-78 ($Tb_{0.5}Gd_{0.5}$) and $\tau_1 = 0.008 \pm 0.0001$ ms and $\tau_2 = 0.07 \pm 0.002$ ms for MIL-78 ($Dy_{0.5}Gd_{0.5}$).

The average lifetime for MIL-78 ($Dy_{0.5}Gd_{0.5}$) was calculated to be 0.0084 ms using the equation: $\tau_{av} = (A_1\tau_1^2 + A_2\tau_2^2)/(A_1\tau_1 + A_2\tau_2)$. The single exponential decay patterns of Eu^{3+} and Tb^{3+} based compounds suggest the existence of a single chemical environment around Eu^{3+} and Tb^{3+}, in agreement with the crystal structure. The bi-exponential decay pattern of the Dy^{3+} based compound suggests the existence of two types of chemical environments around Dy^{3+} which may arise from local structural distortions evoked by the size difference of Dy^{3+} and Gd^{3+}. The emission quantum yields were measured at room temperature using an integrating sphere under the excitation wavelength of 321 nm, yielding luminescence quantum yields of 1.24% for MIL-78 ($Eu_{0.5}Gd_{0.5}$), 19% for MIL-78 ($Tb_{0.5}Gd_{0.5}$), and 0.26% for MIL-78 ($Dy_{0.5}Gd_{0.5}$). The longer lifetime and the higher quantum yield of MIL-78 ($Tb_{0.5}Gd_{0.5}$) compared to other samples can possibly be attributed to the lower number of water molecules in the compound (as evident from the TG data) leading to a smaller contribution from non-radiative decay resulting from the OH oscillation of water molecules.

Moreover, the energy level match between the triplet state of the ligand (BTC^{3-}) and the emissive energy level of the Ln^{3+} ions is an important factor which can affect the emission efficiency of the lanthanide complexes. The triplet level of the ligand needs to be higher than the emissive lanthanide cation level, ideally relatively close, but not too close that energy back transfer processes dominate. According to empirical rules established by Latva, an ideal ligand to metal transfer process occurs when the energy gaps between the ligand and the emissive level of lanthanides are larger than 2000–2500 cm^{-1} for Eu^{3+} and Tb^{3+}.[35] The triplet level of the BTC^{3-} ligand derived from the photoluminescence of Gd-complexes has been deter-

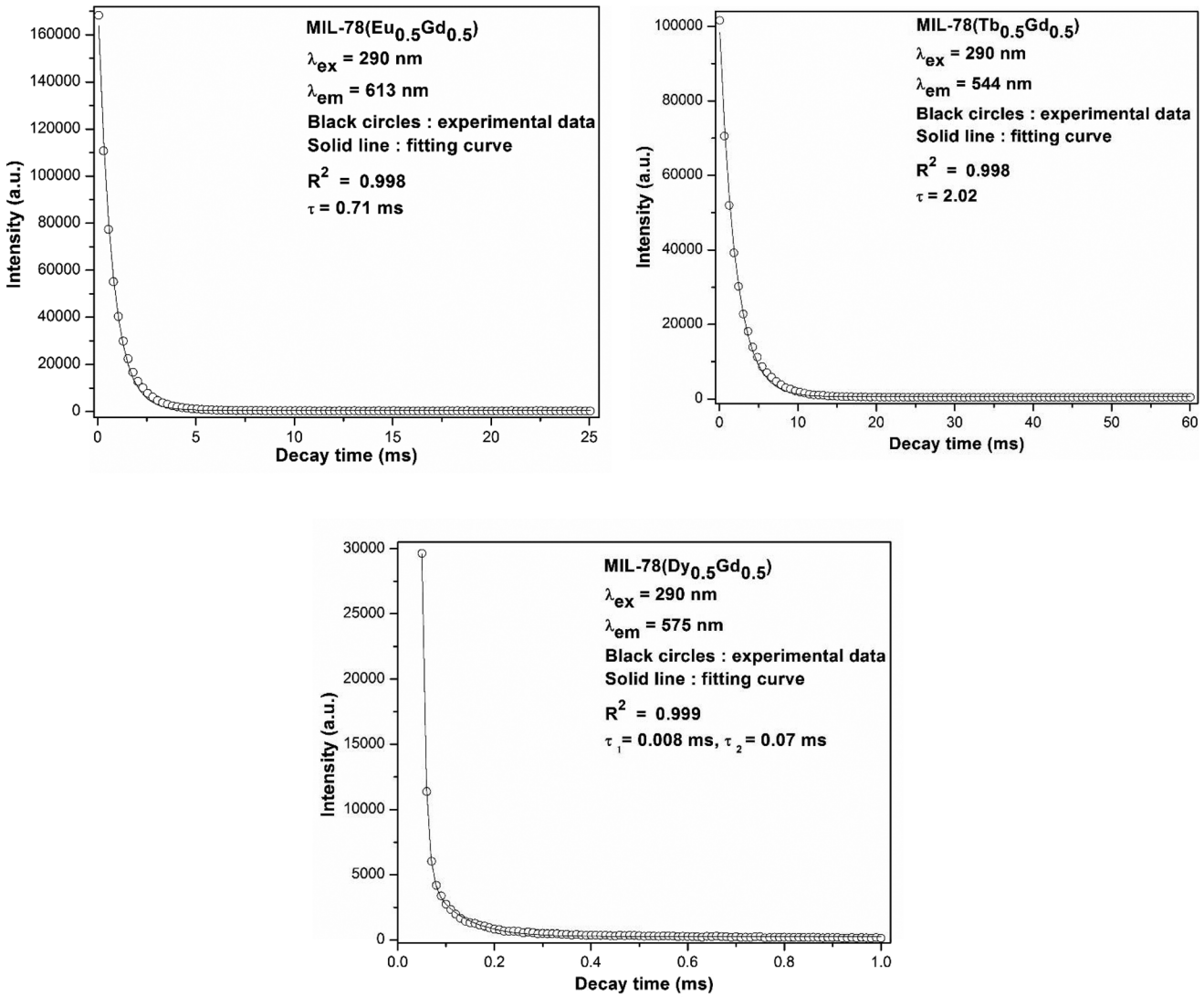

Fig. 8 Room temperature luminescence decay curves of MIL-78 ($Ln_{0.5}Gd_{0.5}$) Ln = Eu, Tb, and Dy.

mined to be at about 23 200 cm^{-1}.[36] At 23 200 cm^{-1} the T_1 energy state of BTC^{3-} is quite higher than that for the $^5D_0$ level of Eu^{3+} (17 300 cm^{-1}), the $^5D_4$ level of Tb^{3+} (20 400 cm^{-1}), and the $^4F_{9/2}$ level of Dy^{3+} (21 000 cm^{-1}).[29,34] The respective energy differences ΔE are 5900 for Eu^{3+}, 2800 for Tb^{3+}, and 2200 for Dy^{3+}. So, the Tb^{3+} based complex shows better luminescence properties than the Eu^{3+} and Dy^{3+} complexes as a result of the good match of the lowest triplet energy level of the BTC^{3-} ligand and the resonance level of Tb^{3+} leading to effective energy transfer from the ligand to the Tb^{3+} ions compared to other Ln^{3+} ions. In general, it has been reported that the ΔE that can minimize the inverse energy transition from the Ln^{3+} ions to the ligand is about 2500–3500 cm^{-1}.[37] The energy difference of the $^4F_{9/2}$ level of Dy^{3+} and the BTC^{3-} triplet state is complex and less than the optimal value, therefore it can be expected that there exists a back transfer process leading to weak luminescence properties. Furthermore, the weak luminescence of MIL-78 ($Dy_{0.5}Gd_{0.5}$) can be ascribed to a small band gap that is more prone to nonradiative deactivation,[38] especially in the case of a high water content.

Conclusions

The luminescence properties of three lanthanide-containing metal–organic frameworks with a MIL-78 structure (MIL-78 ($Ln_{0.5}Gd_{0.5}$) Ln = Eu, Tb, and Dy) prepared by solvent-free ball milling from carbonates of the corresponding lanthanides and benzene 1,3,5-tricarboxylic acid were determined. The three different optically active Ln^{3+} ions Eu^{3+}, Tb^{3+} and Dy^{3+} can be highly sensitized by the BTC^{3-} ligand because the resonance levels of the Ln^{3+} ions are suitably located with respect to the T-level of the ligand. The lifetime varies from 0.71 ms for MIL-78 ($Eu_{0.5}Gd_{0.5}$) to 2.02 ms for MIL-78 ($Tb_{0.5}Gd_{0.5}$) to 0.0084 ms for MIL-78 ($Dy_{0.5}Gd_{0.5}$) and the quantum yields range from 0.2% for MIL-78 ($Dy_{0.5}Gd_{0.5}$) to 19% for MIL-78 ($Tb_{0.5}Gd_{0.5}$). The enhanced

luminescence properties of the Tb-containing MIL-78 MOF can be attributed to a good match of the lowest triplet energy level of the BTC^{3-} ligand with the emissive level of Tb^{3+}.

Conflicts of interest

There are no conflicts to declare.

Acknowledgements

Ames Laboratory is operated for the U.S. Department of Energy (DOE) by the Iowa State University of Science and Technology under contract no. DE-AC02-07CH11358. Research on mechanochemical synthesis and structural characterization was supported by the Division of Materials Sciences and Engineering of Basic Energy Sciences Program of the Office of Science of the U.S. Department of Energy. Research on optical properties was supported by the NSF, grant CHE-1465071.

Notes and references

1 M. P. Suh, H. J. Park, T. K. Prasad and D. W. Lim, *Chem. Rev.*, 2012, **112**, 782–835.
2 S. K. Henninger, H. A. Habib and C. Janiak, *J. Am. Chem. Soc.*, 2009, **131**, 2776–2777.
3 M. Yoon, R. Srirambalaji and K. Kim, *Chem. Rev.*, 2012, **112**, 1196–1231.
4 Y. Cui, Y. Yue, G. Qian and B. Chen, *Chem. Rev.*, 2012, **112**, 1126–1162.
5 W. P. Lustig, S. Mukherjee, N. D. Rudd, A. V. Desai, J. Li and S. K. Ghosh, *Chem. Soc. Rev.*, 2017, **46**, 3242–3285.
6 W. P. Lustig, F. Wang, S. J. Teat, Z. Hu, Q. Gong and J. Li, *Inorg. Chem.*, 2016, **55**, 7250–7256.
7 N. Stock and S. Biswas, *Chem. Rev.*, 2011, **112**, 933–969.
8 J. Klinowski, F. A. A. Paz and J. Rocha, *Dalton Trans.*, 2011, **40**, 321–330.
9 U. Mueller, H. Puetter, M. Hesse and H. Wessel, BASF Aktiengesellschaft, *WO* 2005/049892, 2005.
10 D. Tranchemontagne, J. Hunt and O. M. Yaghi, *Tetrahedron*, 2008, **64**, 8553–8557.
11 T. J. Friščić, *Mater. Chem.*, 2010, **20**, 7599–7605.
12 (*a*) T. Friščić, *Chem. Soc. Rev.*, 2012, **41**, 3493–3510; (*b*) K. Užarević, T. C. Wang, S.-Y. Moon, A. M. Fidelli, J. T. Hupp, O. K. Farha and T. Friščić, *Chem. Commun.*, 2016, **52**, 2133–2136; (*c*) M. Klimakow, P. Klobes, A. F. Thunemann, K. Rademann and F. Emmerling, *Chem. Mater.*, 2010, **22**, 5216–5221; (*d*) D. Prochowicz, K. Sokołowski, I. Justyniak, A. Kornowicz, D. Fairen-Jimenez, T. Friščić and J. Lewiński, *Chem. Commun.*, 2015, **51**, 4032–4035; (*e*) S. L. James, C. J. Adams, C. Bolm, D. Braga, P. Collier, T. Friščić, F. Grepioni, K. D. M. Harris, G. Hyett, W. Jones, A. Krebs, J. Mack, L. Maini, A. G. Orpen, I. P. Parkin, W. C. Shearouse, J. W. Steed and D. C. Waddell, *Chem. Soc. Rev.*, 2012, **41**, 413–447.
13 D. Yuan, G. S. Yi and G. M. Chow, *J. Mater. Res.*, 2009, **24**, 2042–2050.
14 J. McKittrick and L. E. Shea-Rohwer, *J. Am. Ceram. Soc.*, 2014, **97**, 1327–1352.
15 C. Serre, F. Millange, C. Thouvenot, N. Gardant, F. Pellé and G. Férey, *J. Mater. Chem.*, 2004, **14**, 1540–1543.
16 F. Pellé, S. Surblé, C. Serre, F. Millange and G. Férey, *J. Lumin.*, 2007, **122**, 492–495.
17 W. Liu, K. Zhu, S. J. Teat, B. J. Deibert, W. Yuan and J. Li, *J. Mater. Chem. C*, 2017, **5**, 5962–5969.
18 N. K. Singh, M. Hardi and V. P. Balema, *Chem. Commun.*, 2013, **49**, 972–974.
19 N. K. Singh, S. Gupta, V. K. Pecharsky and V. P. Balema, *J. Alloys Compd.*, 2017, **696**, 118–122.
20 R. Vercaemst, D. Poelman, L. Fiermans, R. L. Van Meishaeghe, W. H. Laflere and F. Cardon, *J. Electron Spectrosc. Relat. Phenom.*, 1995, **74**, 45–56.
21 S. Kumar, R. Prakash, R. J. Choudhary and D. M. Phase, *Mater. Res. Bull.*, 2015, **70**, 392–396.
22 F. Mercier, C. Alliot, L. Bion, N. Thromat and P. Toulhoat, *J. Electron. Spectrosc. Relat. Phenom.*, 2006, **150**, 21–26.
23 W. Cartas, R. Rai, A. Sathe, A. Schaefer and J. F. Weaver, *J. Phys. Chem. C*, 2014, **118**, 20916–20926.
24 K. G. Tshabalala, I. M. Nagpure, H. C. Swart, O. M. Ntwaeaborwaa, S.-H. Cho and J.-K. Park, *J. Vac. Sci. Technol., B*, 2012, **30**, 031401.
25 D. Barreca, A. Gasparotto, A. Milanov, E. Tondello, A. Devi and R. A. Fischer, *Surf. Sci. Spectra*, 2007, **14**, 52–59.
26 L. Song and M. Rongjun, *J. Cryst. Growth*, 1996, **169**, 190–192.
27 B. Vallina, J. D. Rodriguez-Blanco, A. P. Brown, J. A. Blanco and L. G. Benning, *J. Nanopart. Res.*, 2013, **15**, 1438.
28 A. Sungur and M. Kizilyalli, *J. Less-Common Met.*, 1983, **93**, 419–423.
29 E. Souza, I. Silva, E. Teotonio, M. Felinto and H. Brito, *J. Lumin.*, 2010, **130**, 283–291.
30 S. Maiti, A. Pramanik, U. Manju and S. Mahant, *ACS Appl. Mater. Interfaces*, 2015, **7**, 16357–16363.
31 C. Chaitanya, *Spectrochim. Acta, Part A*, 2012, **86**, 159–173.
32 G. Jin, Z. Liu, H. Sun and Z. Tian, *Luminescence*, 2016, **31**, 190–194.
33 D. Yang, Y. Tian, W. Xu, X. Cao, S. Zheng, Q. Ju, W. Huang and Z. Fang, *Inorg. Chem.*, 2017, **56**, 2345–2353.
34 H. Zhang, R. Fan, W. Chen, X. Zheng and Y. Yang, *J. Lumin.*, 2013, **143**, 611–618.
35 M. Latva, H. Takalo, V. Mukkala, C. Matachescu, J. Rodriguez-Ubis and J. Kankare, *J. Lumin.*, 1997, **75**, 149–169.
36 W. Yan, L. Wang, K. Yangxio, Z. Fu and T. Wu, *Dalton Trans.*, 2016, **45**, 4518–4521.
37 S. Biju, D. B. Ambili Raj, M. L. P. Reddy and B. M. Kariuki, *Inorg. Chem.*, 2006, **45**, 10651–10660.
38 V. Eliseeva and J.-C. Bünzli, *Chem. Soc. Rev.*, 2010, **39**, 189–227.